Volume 252, No. 13, 30 April 2006 ISSN 0169-4332

Available online at www.sciencedirect.com
SCIENCE DIRECT
Applied Surface Science 252 (2006) 4838–4844
applied surface science
www.elsevier.com/locate/apsusc

Laser impulse coupling at 130 fs

C. Phipps [a,*], J. Luke [a,b], D. Funk [c], D. Moore [c], J. Glownia [c], T. Lippert [d]

[a] *Photonic Associates, 200A Ojo de la Vaca Road, Santa Fe, NM 87508, USA*
[b] *NMT Institute for Engineering Research and Applications, 901 University Blvd. SE, Albuquerque, NM 87106-4339, USA*
[c] *Los Alamos National Laboratory, P.O. Box 1663, Los Alamos, NM 87545, USA*
[d] *Paul Scherrer Institut, CH-5232 Villigen PSI, Switzerland*

Received 3 May 2005; accepted 15 July 2005
Available online 2 November 2005

Abstract

We measured the momentum coupling coefficient C_m and laser-generated ion drift velocity and temperature in the femtosecond (fs) region, over a laser intensity range from ablation threshold to about one hundred times threshold. Targets were several pure metals and three organic compounds. The organic compounds were exothermic polymers specifically developed for the micro-laser plasma thruster, and two of these used ''tuned absorbers'' rather than carbon particles for laser absorption. The metals ranged from Li to W in atomic weight. We measured time of flight (TOF) profiles for ions. Specific impulse reached record values for this type of measurement and ablation efficiency was near 100%. These measurements extend the laser pulsewidth three orders of magnitude downward in pulsewidth relative to previous reports. Over this range, we found C_m to be essentially constant. Ion velocity ranged from 60 to 180 km/s.

PACS: 32.80.Rm; 52.50.Jm; 52.38.Dx; 52.38.Hb; 52.38.Kd; 52.38.Mf

Keywords: Femtosecond; Laser momentum coupling; Lithium; Tungsten; Gold; Optimum coupling fluence; Ion time of flight

1. Introduction: need for fs data in laser ablation propulsion

Knowledge of two parameters is critical for designing successful laser space propulsion applications [1,2]. The first of these is the so-called laser momentum coupling coefficient C_m (N s/J) = J/W which is the ratio of momentum J transferred to an object by laser ablation and the incident laser energy W. The second is the optimum coupling fluence Φ_{opt} (J/m^2) for which C_m is maximized, and this is a critical parameter because the fluence range for optimum coupling is fairly narrow. In particular, the leading-edge slope of an experimental plot of C_m versus Φ is very steep, corresponding to the onset of intense vapor generation. C_m then rises to a maximum at the vapor–plasma transition and decreases somewhat less rapidly at higher laser pulse fluence due to plasma shielding. Fig. 1 shows data [3] which illustrates this point. For applications such as the ORION laser-space-debris clearing concept [1], for which laser systems with tens of kilowatt average power have been proposed, an incorrect value of Φ_{opt} can affect system design and cost unfavorably, or make the whole concept unworkable because correcting the error runs into other limitations such as reaching the threshold for stimulated Raman scattering (SRS) in the atmosphere. Isolated measurements of C_m or ablation rate alone are not sufficient; rather, a clear experimental demonstration that the C_m versus Φ maximum has been achieved is required, and this has not often been done in the literature. In the range 100 ps $< \tau <$ 1 ms, we have shown [2] that Φ_{opt} varies approximately as predicted by 1-D thermal transfer theory [4]:

$$\Phi_{opt}\,(\mathrm{J/m^2}) = B\,\tau^m \tag{1}$$

with $m = 0.5$ and $B = 480$ MJ/m^2. However, the precise result is material-, wavelength- and pulsewidth-dependent and, previous to this work, information on Φ_{opt} and the associated C_m did not exist for pulses shorter than 100 ps, and no proven model

* Corresponding author. Tel.: +1 505 466 3877; fax: +1 505 466 3877.
E-mail address: crphipps@aol.com (C. Phipps).

0169-4332/$ – see front matter © 2005 Elsevier B.V. All rights reserved.
doi:10.1016/j.apsusc.2005.07.079

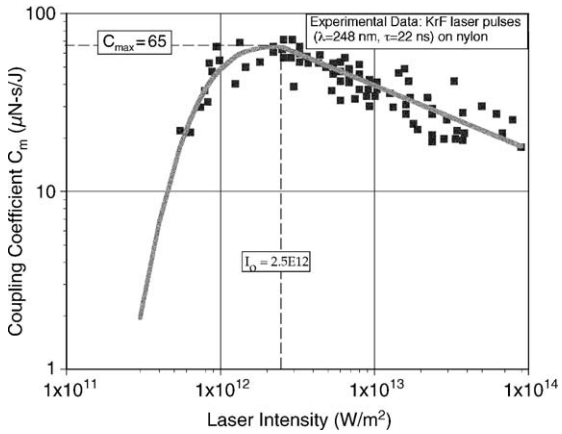

Fig. 1. Data illustrating the concept of optimum coupling fluence. In this case, the optimum intensity is 2.5 TW/m^2 and Φ_{opt} = 55 kJ/m^2.

existed for predicting the parameters. Yet, interesting applications for femtosecond-pulse momentum transfer exist.

Aside from these practical concerns, a second motivation for this work was to discover where the short-pulse breakdown would occur in our theoretical model [3,5] for C_m, exhaust velocity v_E, electron density n_e and temperature T_e in the range 100 ps $< \tau <$ 1 ms. In particular, the authors of ref. [6] have shown that this breakdown point is probably τ = 10 ps. Specific impulse is defined by the relationship $I_{sp} = v_E/g_o$, where g_o is the standard acceleration of gravity at sea level.

2. Experimental setup

Fig. 2 shows the setup we used for these measurements. For the ablation laser, pulse duration was 130 ± 10 fs, wavelength was 800 ± 5 nm and maximum pulse energy was 20 mJ. As appropriate, reflective and absorptive attenuators were used to vary pulse energy on the target over a factor of 20, and three different laser spot sizes were used. Combining both effects, fluence on target could be varied through nearly two orders of magnitude.

To generate useful physics data, we were careful to make target size closely match laser beam size on the target. Targets which are larger than the beam spacially integrate the expanding blast wave, adding momentum which is geometry-dependent rather than a basic property of the interaction. Targets 4.0 and 1.0 mm in diameter were used with beam diameters at $1/e^2$ intensity of 3.4 and 1.1 mm, respectively. A third beam diameter of 0.56 mm was also used. For data generated in this configuration, C_m was adjusted downward for the spacial integration referred to above, using an approximate technique described in the next section. This correction was of order 25%. Beam distributions were measured using the varying intensity fixed threshold method [7]. The ablation laser was incident at 22° on plane, circular targets. Polarization was *s*-plane, but the near-normal angle of incidence makes the polarization state of mainly academic interest.

Impulse was measured using a torsion pendulum [2] to which the target was mounted with vacuum grease. Its response was 6.81 μN s/rad, and the response was read out using a probe beam reflecting off a mirror mounted to its center of rotation. The resonant frequency of the pendulum was measured for each target and used to adjust the basic pendulum calibration for varying target mass using a technique described in ref. [2]. The nature of the impulse sensor limited us to single shot measurements. Targets were manually aligned to ±100 μm transverse accuracy to the incident beam footprint (Fig. 3). Nevertheless, alignment errors were responsible for scatter in the results obtained. A high-magnification video telemicroscope facilitated transverse alignment, and the microscope's 10 μm depth of field facilitated axial positioning of the target on the torsion pendulum in the converging laser beam.

Typical target chamber pressure was 1.3×10^{-2} Pa.

Ion time of flight (TOF) data was taken for each shot, using a Burle Instruments TOF detector with a two-stage microchannel plate (MCP) at the end of a 116-cm field-free drift tube. MCP voltage varied from 1250 to 1900 V depending on the ion flux.

As many as 20 shots were taken on each target before replacement, since single shot etch depth was only a few nanometers. Typically, five surface-cleaning shots were applied to remove debris and traces of surface grease before data were recorded. A total of 204 impulse data shots were taken on 10 materials. These were Li, Al, Mo, Fe, Zr, Au, W, and three energetic polymers which are of interest for the microthruster work, and which are described in detail in ref. [8]. Two of the polymers were doped with a tuned IR absorber centered at 915 and 935 nm, respectively, wavelengths appropriate for the microthruster application [2]. The third used nanodisperse carbon as the laser absorber.

Metallic targets were all certified to have purity better than 99.95% by their supplier, Alfa-Aesar. The organic targets were prepared as indicated in ref. [8], and used polyimide substrates.

Targets were mounted on both arms of the torsion pendulum to maximize data throughput per vacuum-to-air cycle.

3. Accounting for oversize targets

To generate good physics data from the one case (highest intensity points in tungsten data) in which target diameter was 1.1 mm and the laser beam spot diameter 0.56 mm, it was necessary to take account of the additional impulse produced as the blast wave rolls out across regions of the target beyond the laser beam diameter (Fig. 4).

Target radiation is ignored, an adiabatic expansion from the initial pillbox of thickness $w = \lambda$ is assumed, expanding at velocity v to cover a diameter $D(t) = D_o + 2vt$, and we approximate the expanded volume $V(t)$ by

$$V(t) = \left(\frac{\pi}{4}\right)(w + 2vt)D^2 \tag{2}$$

$$\text{with} \quad V_o = \frac{\pi D_o^2 w}{4}. \tag{3}$$

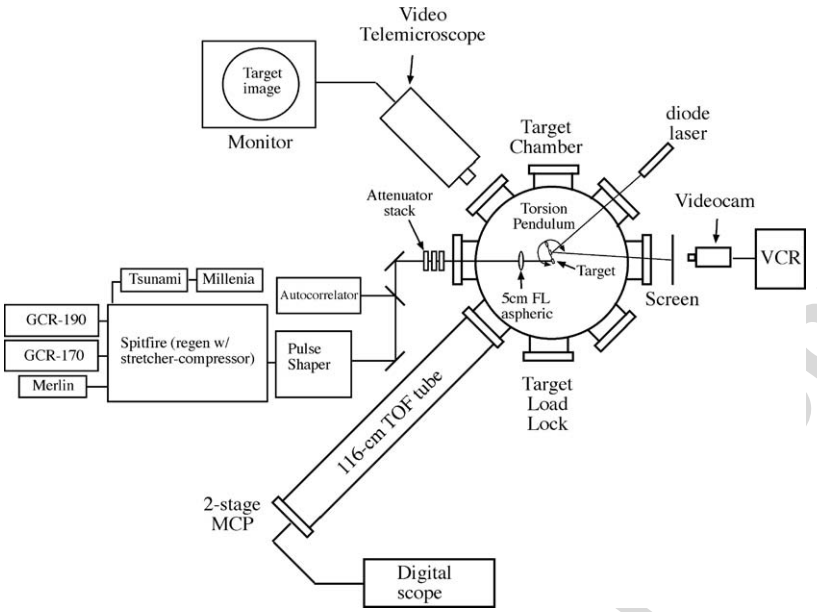

Fig. 2. Experimental setup for the fs measurements. Pulse energy of 20 mJ was available at 130 fs. Three sizes of target were used to match three different focal spot sizes, which were obtained by careful positioning of the target on the torsion pendulum in the converging laser beam using the 10 μm depth of field of a high-magnification video telemicroscope.

Then, with $b = 2v/D_o$, $c = 2v/w$, we have

$$\left(\frac{P}{P_o}\right) = \left(\frac{V_o}{V}\right)^{\gamma} = (1+ct)^{-\gamma}(1+bt)^{-2\gamma}. \quad (4)$$

Defining

$$F_1 = (1+ct)^{-\gamma} \quad (5)$$

and

$$F_2 = (1+ct)^{-\gamma}(1+bt)^{-2\gamma}, \quad (6)$$

where t_1 is the time at which $D = D_o$,

$$t_1 = \frac{D_o}{(2v)} \quad (7)$$

and t_2 is the time at which $D = D_t$,

$$t_2 = \frac{(D_t - D_o)}{(2v)} \quad (8)$$

$$bt_2 = \left(\frac{D_t}{D_o - 1}\right), \quad (9)$$

After some manipulation, we find an approximate correction factor C for the measured C_m

$$C = \frac{\int_0^{t_1} F_1(t)\,dt + \int_{t_1}^{\infty} F_2(t)\,dt}{\int_0^{t_2} F_1(t)\,dt + \left(1 + \frac{D_t^2}{D_o^2}\right)\int_{t_2}^{\infty} F_2(t)\,dt} \quad (10)$$

In Eq. (10), the numerator is the impulse J_m that would be applied to a matched target with $D_t = D_o$, while the denominator

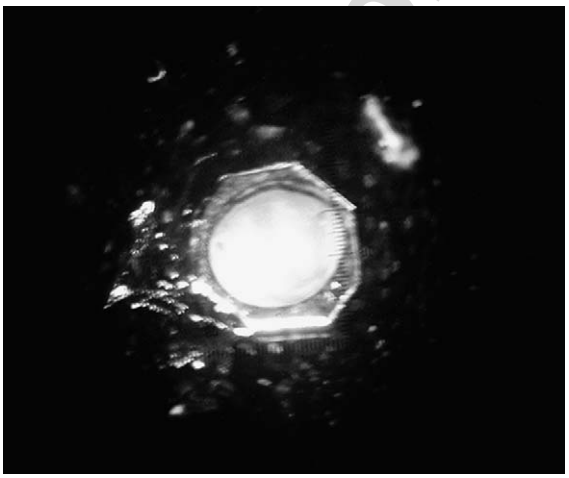

Fig. 3. Successful target alignment with a 1-mm target. The bright area in the center of the target is the result of about 20 shots.

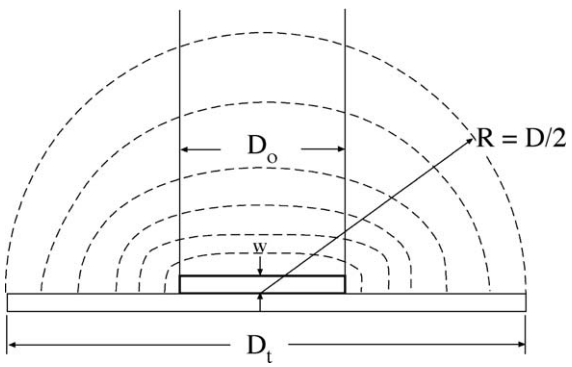

Fig. 4. Target interaction geometry for the discussion in Section 3. Target diameter D_t is considerably larger than incident beam diameter D_o. Beam energy is deposited in a pillbox of thickness $w = \lambda$, and the blastwave subsequently expands across the target.

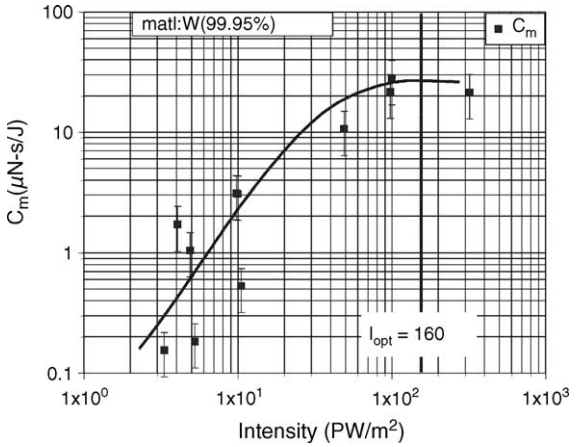

Fig. 5. Impulse coupling data for tungsten, giving $\Phi_{opt} = 21$ kJ/m^2.

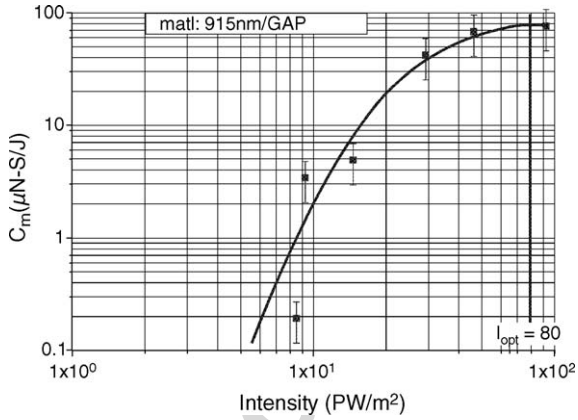

Fig. 6. Impulse coupling data for the energetic polymer gliycidyl azide polymer (GAP) doped with IR absorber tuned to 915 nm, giving $\Phi_{opt} = 10$ kJ/m^2.

is $(J_m + J_\Delta)$, J_Δ being the impulse that is applied to the target annulus outside the matched region. For our conditions, $D_o = 0.56$ mm, $D_t = 1.1$ mm and using $v = 25\,\mathrm{km/s}$, we find $C = 0.76$.

4. Results

4.1. Momentum coupling data

Figs. 5 and 6 show examples of impulse coupling results we obtained for one metal and one organic target. To reduce scatter, the impulse from five single shots at the same intensity were numerically averaged to obtain one data point in the plot. The error bars show the range of the original data. A curve was drawn through the data to guide the eye, and the corresponding intensity for maximum impulse coupling efficiency, I_{opt}, indicated on each plot. Only a factor of 2 difference is seen between the optimum coupling intensity for these two materials.

These new data points are then presented on the revised optimum fluence plot, Fig. 7. All results are summarized in Table 1. In the table, maximum exhaust velocity is drawn from the TOF data which will be discussed in the next section.

4.2. Time of flight data

Although originally planned as a secondary measurement, the TOF data turned out to be at least as interesting as the primary momentum transfer data. Sometimes, the data demonstrated a single, high velocity peak. More often, there were two or even three peaks (Fig. 8). In general, all the ion peaks could be fit reasonably well by a drifting thermal Maxwellian.

In Fig. 9, we have plotted the most probable thermal velocity (where k is Boltzmann's constant, and T_e and m_e are, respectively, the electron temperature and mass) which is given by

$$v_{th(p)}\,(\mathrm{cm/s}) = \left(\frac{2kT_e}{m_e}\right) = 1.385 \times 10^6 \left(\frac{T_{eV}}{A}\right)^{1/2} \qquad (11)$$

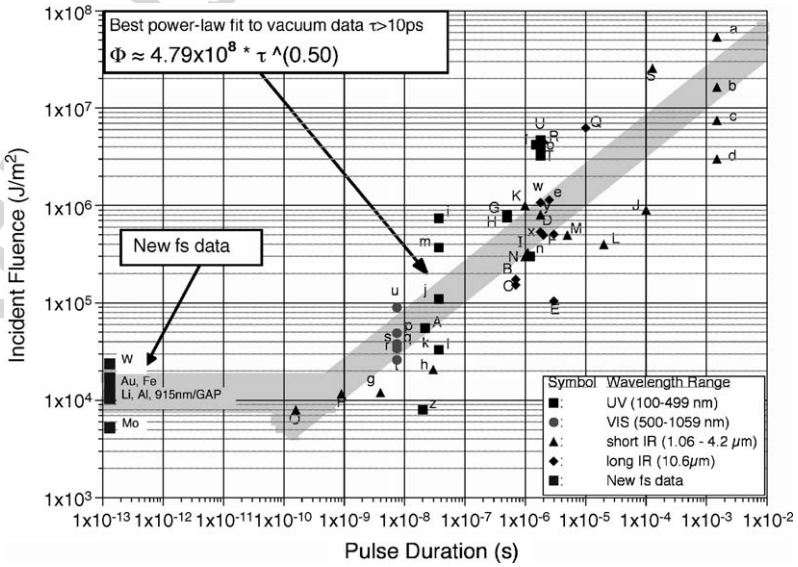

Fig. 7. Optimum coupling fluence plot shows purely thermal behavior down to 100 ps, and a flat behavior for shorter pulses. Our data is at the extreme left. Letters next to data points in the figure are references to the literature explained in ref. [2].

Table 1
Experimental results

Material	Φ_{opt} (kJ/m^2)	Experimental C_{mopt} (μN/W)	Ref. [3] model C_m (μN/W)	Ref. [3] model v_i (km/s)	Fast ion drift velocity (km/s)	Slow ion drift velocity (km/s)	Slow ion I_{sp} (s)
Li	10.4	25	20	41	180	23	2350
Al	11.7	18	36	23	150	22	2245
Mo	5.2	42	62	13	130	24	2450
Au	16.9	20	85	9.4	160	24	2450
Fe	13.0	35	49	16	140	22	2245
W	20.8	30	82	9.7	110	31	3160
915 nm IR absorber	10.4	80	25	32	68	20	2040
935 nm IR absorber	13.0	32	25	32	100	32	3265
C:GAP	13.0	40	25	32	57	37	3775

versus atomic mass A, rather than the temperatures of the ions in the hot, warm and cold peaks in order to highlight the fact that this quantity is nearly constant across the large range of atomic mass studied. The only parameters which change much over the range are $v_{th(p)fast}$ and $v_{th(p)slow}$, which decrease by a factor of 2 as we go from Li to W targets. Fig. 10 shows the variation of TOF parameters versus intensity, for gold. Fig. 11 demonstrates the good correlation between ion flux and measured momentum versus incident intensity.

We found that impulse measured with the torsion pendulum was highly correlated with measured total ion flux over a decade in laser intensity (Fig. 11). There are undoubtedly a lot of neutrals, clusters, etc., in the ablation plume, but their contribution to total momentum is not as significant as that of the ions, and we conclude that they have low velocity relative to that of the ions.

5. Discussion

Measured impulse coupling coefficients differ by as much as a factor of 5 relative to the ref. [3] prediction using $Z = 1$ at 130 fs. This substantiates the ref. [6] claim that the ref. [3] theory begins to fail for pulses shorter than about 10 ps.

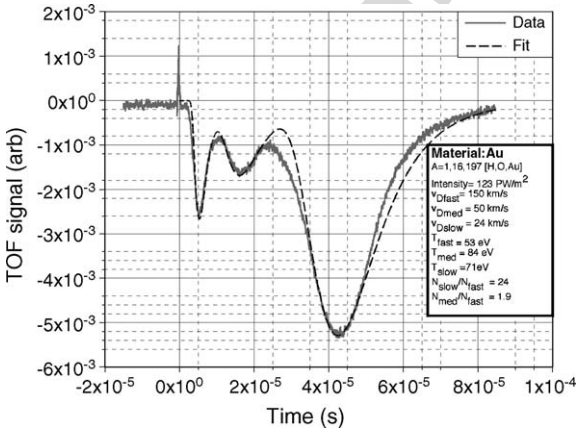

Fig. 8. TOF data for gold, fit by individual drifting Maxwellians. Drift velocities are 155, 0.55 and 0.26 km/s, respectively, for what we assume to be hydrogen, oxygen and gold ions. Temperatures for the three groups are 53, 84 and 71 eV, respectively.

Since mass analysis was not available for these measurements, there is some uncertainty in assigning identity to the ion peaks. The slow ion peak velocity is about 50% larger than that predicted by ref. [3]. The fast ion temperature we derive from the data fit in Fig. 9 is 10.4 keV if we assume the ''fast'' peak is due to Au, but only 53 eV if we assume it is due to H. This value is consistent with the temperatures derived for the ''medium'' and ''slow'' peaks, assuming the ''medium'' peak is due to oxygen. Similar results were obtained for the other target materials (Table 1). We therefore take the fast ion peak to be due to hydrogen ions, and the medium velocity (''med'') peak which is sometimes seen, as due to oxygen, arising from water. The specific impulse values are not dramatically different from what one sees in ns-pulse work, or even [9] at 20 ns.

Others have seen similar multiple peaks in TOF measurements. Ye and Grigoropoulous from the Russo group at Lawrence Berkeley Laboratory [10] studied laser ablation of Ti at 80 fs and intensities similar to ours, and found 2–3 ion peaks with a fast ion drift velocity $v_{Dfast} \sim 2 \times 10^7 cm/s$. Over a decade of incident intensity, v_{Dfast} varied less than a factor of 2.

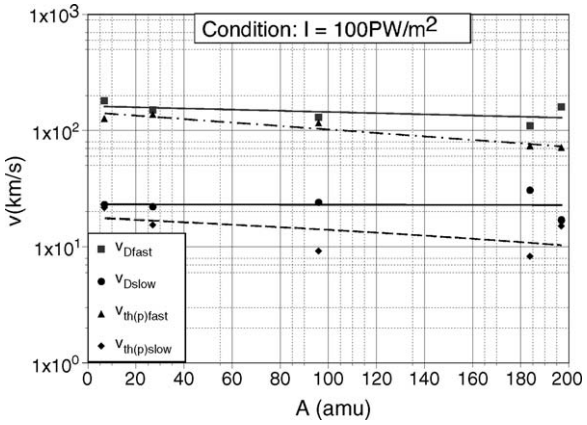

Fig. 9. Variation of TOF ion parameters with atomic mass A, at 10 TW/cm^2. Targets were Li, Al, Mo, Fe, Zr, Au and W. Here, we plot $v_{th(p)slow}$ (the most probable thermal velocities) rather than T_{slow} and to eliminate the atomic mass dependence of the temperatures, which distracts from the point we wish to make. Only a slight variation of the ion velocities is seen. As atomic mass increases by a factor of 29, and $v_{th(p)slow}$ decreases according to $A^{-0.21}$, and v_{Dfast} is nearly constant.

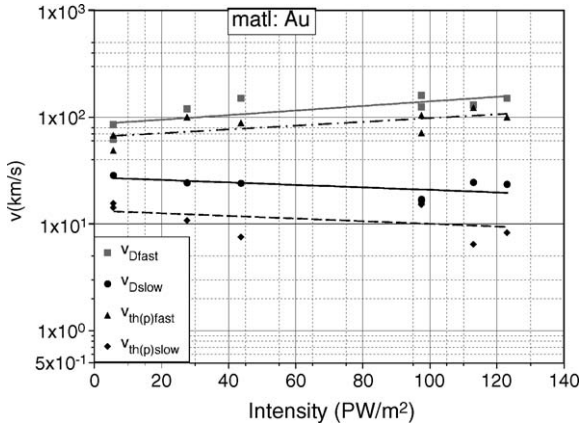

Fig. 10. Variation of TOF ion parameters with intensity for gold. Only a slight variation is seen. Over a factor of 20 in incident intensity, T_{slow} decreases by a factor of 2 according to $I^{-0.25}$ and v_{Dslow} by a factor of 1.4, as $I^{-0.11}$.

They appeal to Coulomb explosion as the source of the first peak. Features very similar to those we report were observed on Ti using a much lower base pressure (1×10^{-5} Pa) and a 3 Hz shot rate.

Amoruso et al. [11,12] reported double peaks from Au, Cu and Al illuminated by 120 fs pulses, also around 100 PW/m^2. They noted the presence of H ions, and did do mass analysis, which showed that the hydrogen content never exceeded a few percent of the collected ion yield. They found p-polarized light to be about 10 times more effective than s-polarized light in generating ions. However, with their 50° incidence angle, the distinction between polarization states is expected to be much more significant than in our case.

Varel et al. [13] made measurements on sapphire with 200 fs pulses at up to 2 TW/cm^2. Using a time of flight mass spectrometer, Al^+, O^+ and O^{2+} ions were observed. They consider a two-step process in which Coulomb explosion from

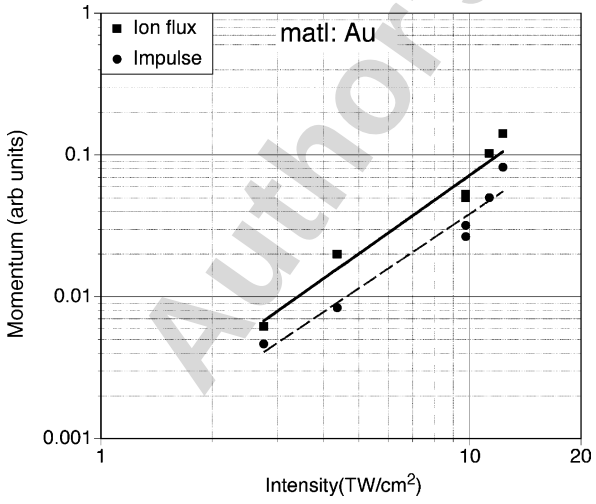

Fig. 11. The variation of ion flux and measured momentum transfer show good correlation over a decade in laser intensity. There are undoubtedly a lot of neutrals, clusters, etc. but their contribution to total momentum is not as significant as that of the ions.

ionized defect centers drives the first peak, followed by a thermal ion pulse which transports the bulk of neutral ablated material.

Pakhomov et al. [14] made measurements of ion velocities generated by a number of materials at 100 fs. They saw ion drift velocities decrease approximately according to $A^{-0.5}$, whereas our measurements showed v_{Dfast} and v_{Dslow} nearly independent of A. The difference in results may be due to our being far above thermal ablation onset intensity, and also to their high base pressure of 0.4 Pa, a pressure for which the mean free path for ion collision with neutrals is in the order of 5 cm.

We can say that the drift and thermal velocities we observed are nearly constant versus atomic mass A for all materials at 100 PW/m^2, and do not depend much on intensity either, for a single material. This rather unexpected result indicates a fast-peak acceleration process which emphasizes momentum conservation rather than energy conservation in the mechanism connecting the incident photons with accelerated charged particles leaving the target. Even more surprising is the opposite trend of both velocities and temperatures versus intensity between the hot and cold distributions.

Examples of momentum-conserving processes are Coulomb explosion, as well as wave–wave interactions in a plasma, e.g., stimulated Raman scattering. However, Bulgakova et al. have stated that theory predicts Coulomb explosion to be impossible for metals [15] because their higher electrical conductivity inhibits build-up of the required accelerating field. SRS produces an electron plasma wave with frequency ω_{epw} given by

$$\omega_o = \omega_s + \omega_{epw} \tag{12}$$

where ω_s is the frequency of the scattered optical wave. This process has often been observed in inertial confinement fusion (ICF), and has an intensity threshold that depends linearly on the density gradient $\Delta n/\Delta x$, and involves the critical electron density $n_{ec} = 1.115 \times 10^{27}/\lambda^2_{o\,(\mu m)}$ and the ubiquitous ICF scaling parameter $I\lambda^2_{o\,(\mu m)}$ (where by $\lambda_{o\,(\mu m)}$ we denote the incident wavelength in micrometers). According to ref. [16], this threshold is given by:

$$I\lambda^2_{o(\mu m)} \cdot 5 \times 10^{21} \left(\frac{n_{ec}}{\langle n \rangle}\right)^2 \cdot \left(\frac{\Delta n}{n_{ec}}\right)\left(\frac{\lambda_o}{\Delta x}\right) \tag{13}$$

A reflected wave of frequency $\omega_o/2$ is generated, plus a cascade of forward-going waves at frequencies $\omega_o \pm n\text{-}\omega_{epw} \approx \omega_o \pm n\omega_o/2$ because gain for the process maximizes at 1/4 critical density. These waves heat a finite number of electrons to very high energy. Simulations show that the heated temperature is roughly independent of intensity, depending mainly on the density and background temperature, which in turn control the phase velocity of the Raman-generated plasma wave. These heated electrons then will (a few picosecond later) strip enough ions from the target surface to produce charge

neutrality, dragging them along with a velocity that depends only on this initial, fixed temperature.

However, to match the conditions indicated in Eq. (13), we need a large gradient scale length Δx of order $800\lambda_o$, or higher intensity. The former could be achieved by prepulses. The latter could be achieved by filamentation in the plasma. However, we did not have diagnostics capable of revealing the truth of either conjecture.

We found that the measured impulse correlated well with the ion flux, determined by adding contributions from all the peaks. It has been observed by Amoruso et al. via their continuum emission that a slow cloud of nanoparticles are invariably emitted from targets under femtosecond irradiation. This may explain why the specific impulse we determined from ion velocities was at least an order of magnitude higher than that which we determined from target mass loss.

6. Conclusion

We measured optimum impulse generation fluence and associated momentum transfer coefficient at 130 fs on several metals and three organic materials. To our knowledge, this is the first such measurement for pulses shorter than 100 ps. We found the 130 fs optimum coupling fluence to be essentially the same as that for 100 ps. We also measured TOF signals for ions generated in the ablation experiments and found that drift velocities and temperatures changed very little over the intensity range 5–120 PW/m^2 on a particular metal, or over the range from 7 to 200 amu at 100 PW/m^2. Generally, we found two to three peaks in the TOF signal, and that the second peak became more dominant as intensity increased.

We postulated two alternative mechanisms for generation of the fast ion peaks.

Acknowledgments

This work was supported by Photonic Associates' Internal Research and Development Fund. The thoughtful and effective assistance of the Los Alamos co-authors, their many helpful suggestions, and the use of their laser laboratory is very gratefully acknowledged.

References

[1] C.R. Phipps, H. Friedman, D. Gavel, J. Murray, G. Albrecht, E.V. George, C. Ho, W. Priedhorsky, M.M. Michaelis, J.P. Reilly, Laser Part. Beams 14 (1) (1996) 1–44.
[2] C. Phipps, J. Luke, AIAA J. 40 (2) (2002) 310–318.
[3] C. Phipps, T. Turner, R. Harrison, G. York, W. Osborne, G. Anderson, X. Corlis, L. Haynes, H. Steele, K. Spicochi, T. King, J. Appl. Phys. 64 (3) (1988) 1083–1096.
[4] H.S. Carslaw, J.C. Jaeger, Conduction of Heat in Solids, second ed., Clarendon Press, Oxford, 1959, p. 75.
[5] C. Phipps, R. Dreyfus, in: A. Vertes, R. Gijbels, F. Adams (Eds.), Laser Ionization Mass Analysis, Wiley, New York, May 1993, pp. 369–441.
[6] F. Beinhorn, J. Ihlemann, K. Luther, J. Troe, SPIE 5448 (2004) 572–580.
[7] I.M. Winer, Appl. Opt. 5 (1966) 1437–1439.
[8] T. Lippert, M. Hauer, L. Urech, A. Wokaun, E. Schmid, SPIE 5448 (2004) 52–64.
[9] C. Phipps, M. Michaelis, J. Laser Part. Beams 12 (1) (1994) 23–54.
[10] M. Ye, C. Grigoropoulous, J. Appl. Phys. 89 (2001) 5183–5190.
[11] S. Amoruso, X. Wang, C. Altucci, C. de Lisio, M. Armenante, R. Bruzzese, R. Velotta, Appl. Phys. Lett. 77 (2000) 3728–3730.
[12] S. Amoruso, X. Wang, C. Altucci, C. de Lisio, M. Armenante, R. Bruzzese, R. Velotta, Appl. Surf. Sci. 186 (2002) 358–363.
[13] H. Varel, M. Wähmer, A. Rosenfeld, D. Ashkenasi, E. Campbell, Appl. Surf. Sci. 127 (1998) 128–133.
[14] A. Pakhomov, A. Roybal, M. Duran, Ion dynamics of plasmas induced in elemental targets by femtosecond laser radiation, Appl. Spectrosc. 53 (1999) 979–986.
[15] N. Bulgakova, R. Stoian, A. Rosenfeld, W. Marine, E. Campbell, SPIE 5448 (2004) 121–135.
[16] K. Estabrook, W. Kruer, B. Lasinski, Phys. Rev. Lett. 45 (1980) 1399–1403.